IEEE Access
Multidisciplinary | Rapid Review | Open Access Journal

Received December 5, 2019, accepted December 24, 2019, date of publication December 30, 2019, date of current version January 8, 2020.

Digital Object Identifier 10.1109/ACCESS.2019.2962900

Total Harmonic Distortion and Output Current Optimization Method of Inductive Power Transfer System for Power Loss Reduction

JUNKUN ZHANG[1], ZHIXING HE[1], (Member, IEEE), AN LUO[1], (Senior Member, IEEE), YANG LIU[1], GUOZHEN HU[2], XUE FENG[3], AND LEI WANG[1], (Member, IEEE)

[1]College of Electrical and Information Engineering, Hunan University, Changsha 410082, China
[2]College of Electrical and Electronic Information Engineering, Hubei Polytechnic University, Huangshi 435003, China
[3]Engineering Cluster, Singapore Institute of Technology, Singapore 138683

Corresponding author: Zhixing He (hezhixingmail@163.com)

The National Natural Science Foundation of China under Grant 51807057 (Theoretical Research on Key Points of Modular Combined DC Converter for Seafloor Observation Network).

ABSTRACT Inductive power transfer (IPT) system is widely used in material handling. A typical structure of the system takes an H-bridge inverter with an inductor-capacitor-inductor (LCL) resonant filter to realize a constant track current supplying changeless energy to the second side. However, the output voltage total harmonic distortion (THD) of the inverter increases, which causes the increase of output current circulation, when using voltage width control method to eliminate source voltage fluctuating. Therefore, a two-stage converter is proposed to optimize the output current circulation. The two-stage IPT system is composed of a boost converter cascaded with an H-bridge resonant inverter. The boost converter is employed to provide a higher and stable DC bus voltage. The H-bridge resonant inverter operates in a fixed width with a constant switching frequency. With the proposed topology, the THD of the high frequency voltage maintains the minimum value to realize minimum output current circulation in the LCL filter. The soft switching is realized to reduce the losses. Furthermore, expressions of coil and track model are presented by combining the theoretical analysis and finite element analysis (FEA). The experimental results show that over 76.6% efficiency is demonstrated in conditions of an 800 W load at the 14% source voltage fluctuation and the maximum efficiency was 78.6 %. The range of efficiency variation was 2% compared to a full-bridge system with voltage pluse-width control of which was 4.6%.

INDEX TERMS Inductive power transfer (IPT), material handling, THD optimization, soft switching, finite element analysis (FEA).

I. INTRODUCTION

Dynamic IPT system has many characteristics such as safety, convenience, and high efficiency. Furthermore, it can operate in rugged environment with the high reliability, low maintenance cost, and more freedom of motion. An application scenario of typical dynamic IPT system is illustrated in Fig. 1. The automated guided vehicles (AGVs) or transfer cars are dynamically supplied and charged during their moving by the coils undergrounds [1]–[6].

Conventionally, a dynamic IPT system consists of the primary side and the second side shown in Fig. 2.

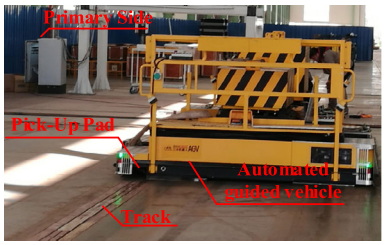

FIGURE 1. Application scenario of dynamic IPT system.

The primary side is composed of rectifier, inverter, and compensation network. It converts the low frequency alternating current (LFAC) to the high frequency alternating current (HFAC) and provides the high frequency energy to the second

The associate editor coordinating the review of this manuscript and approving it for publication was Mouloud Denai.

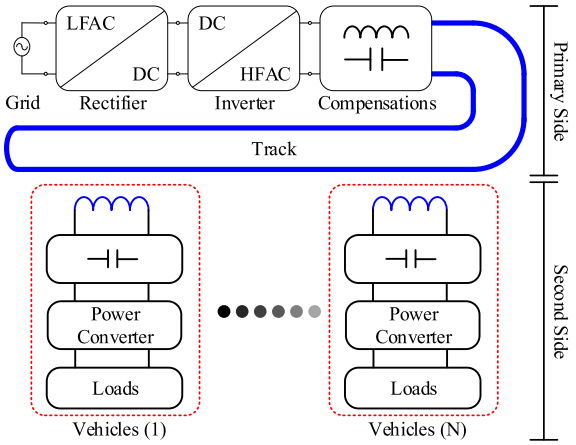

FIGURE 2. Dynamic inductive power transfer system.

TABLE 1. Review of loss reduction progress in dynamic IPT system.

Method	Loss reduction Techniques	Additional components
Increase track current[12]-[15]	Achieve high voltage gain	LCL filters
Leakage inductance compensation[16]-[22]	Reduce system reactive capacity	Capacitance
Inverter soft switching [13], [15]-[17]	Reduce the loss of switch devices	Capacitance and inductance

side through the track current. The second side includes a series of vehicles with pick-up pad and high frequency rectifier. It absorbs the high frequency energy from the track through the pick-up pad [7]–[10].

Inverter is a key component for IPT system shown in Table 2. Class-E IPT system is a promising structure for small power and consumption level to achieve soft switching with high efficiency and frequency [28]–[30]. The switch voltage stress is at least twice of the input voltage. The heat dissipation problem in single switch device also hinder its expansion in medium & high power application. Push-pull IPT system gets attention for its simple structure and high efficiency in IPT application [31]–[33]. However, It needs bigger and costlier inductors compared to capacitances with high-energy storage density. Compared to these IPT systems, H bridge is the most suitable inverter for this application, which has high output voltage, heavy output power, small voltage stress, and small power stress.

Considering the disturbance of source voltage, pulse width modulation (PWM) and pulse frequency modulation (PFM) are the most common way for regulation control. As mentioned early, compensation networks desire working at fixed frequency for leakage inductance compensation. Therefore, PWM based on voltage control with fixed switching frequency is widely used in the IPT systems [23], [24]. Since pulse width modulation method is used to stabilize the current of the track in primary side, the pluse width of the high frequency voltage wave is changed by the H-bridge inverter [23]. Large harmonic voltages are produced when the pulse width of the high frequency voltage changes. At this condition, only the fundamental voltage component can pass through the LCL networks and produces the current in the track, while other harmonic voltage components produce large harmonic currents. These harmonic currents circulate between the H bridge and the LCL network, which cause large circulating reactive power, increase the power loss, and enlarge the voltage and current stresses of the device [24]. [1] mentions the use of two-level structure for optimization, but it rarely mentions how to use the intermediate dc-dc converters for optimization. The H bridge is modulated by the square wave with full duty cycle. Meanwhile, little attention is focused on the optimization of the H-bridge output voltage. In fact, total harmonic distortion (THD) of the high frequency voltage has a minimum value when the width is set as a specific value as derived in the following pages. Then, the output current of the H bridge is optimized with a minimum THD value to improve the efficiency and the reliability of the primary side.

Another challenging work for dynamic IPT system is the design of the pick-up pad. There are many different shapes of pick-up pad shown in the literatures, such as round, rectangular, S- type and E- pick up [34]–[36]. The magnetic circuit, migration, and mechanical structure are analyzed in detail. The mathematical method has been presented in these applications. The rectangular pick-up pad is widely used in material handling. Nevertheless, little analysis of the rectangular pick-up pad is carried out for it with series- and series-compensation in high current and low voltage applications.

The main contributions of this paper are as follows:

1. A new IPT system is proposed for automated guided vehicles (AGVs), which consists of a boost converter cascaded with an LCL filter coupling H-bridge resonant inverter.

TABLE 2. Overview of different IPT system characteristics.

IPT System Types	Cost	Operating frequency	Power level	Applications	Advantages	Disadvantages
Class-E [28]-[30]	Low	>= 200 kHz	Low	Consumer electronics &bio-medical device	Simple & high-efficiency	High voltage stress
Push-Pull [31]-[33]	Medium	< 150kHz	Medium	Single-phase source Consumer electronics	Simple drive	High voltage stress
H-Bridge [1]-[6], [23], [24]	High	< 100kHz	High & Medium	Transportation, AGV & transfer car	Small current and voltage stresses & high power	Relatively high loss

In the proposed system, the boost converter is employed to provide a higher and stable output voltage when the source voltage fluctuates. Due to the constant current characteristics of the LCL filter and the stable output voltage of the boost converter, the H-bridge resonant inverter operates in a constant output voltage width with a constant switching frequency.

2. An output current optimization method, which calculates the minimum THD of the output voltage for decreasing the harmonic current circulation in the H-bridge resonant inverter, is proposed to minimize the output current.

3. Impedance matching methods, which match LCL filter with slight inductance characteristic and the inductor of boost to work in discontinuous current mode (DCM), are used in the proposed system to achieve zero voltage switching (ZVS) in the H bridge and zero current switching (ZCS) in the boost converter.

4. The optimized coil design is proposed through the mathematical analysis and finite element analysis (FEA) based on the coils and track magnetic model, which gets the maximum efficiency with the optimization of coil turns and coil distance.

The remainder of the paper is organized as follows. Section II presents the topology, operation principle and soft switching condition of the proposed two-stage IPT system. Based on these, Section III gives a design approach for this structure. The coupling mechanism is evaluated and optimized by using Biot-savart's law and FEA. Finally, section IV and V present the experimental results, some discussions, and conclusions.

II. PROPOSED CURRENT OPTIMIZATION METHOD

The proposed system consists of two switch-circuit stages defined as the boost regulator stage and the H-bridge resonant inverter stage shown in Fig. 3. The boost converter in the front regulates the voltage V_{dc} of C_{dc} to avoid the influence of the source voltage fluctuation. The H bridge converts the dc voltage into HFAC to the second side through the track current. LCL network including L_{f1}, L_{f2}, and C_f is utilized to filter the high frequency harmonics. Series and series type capacitors C_p and C_s compensate leakage inductances of the track and the pick-up pad. To minimize the harmonic circulation of the H-bridge resonant inverter and LCL network, the H-bridge resonant inverter operates in open loop control mode with a fixed output voltage width. Soft switching of the proposed two-stage IPT system is realized since the boost converter operates in DCM. The constant switching frequency of the H bridge equals the resonant frequency of the LCL resonant network.

A. POWER CIRCULATION OPTIMIZATION WITH MINIMIZED THD

The THD expression of the high frequency voltage is derived, and it finds that the THD has a minimum value when the width is set as a specific value. Therefore, the output voltage of the H bridge is optimized with a minimum THD value

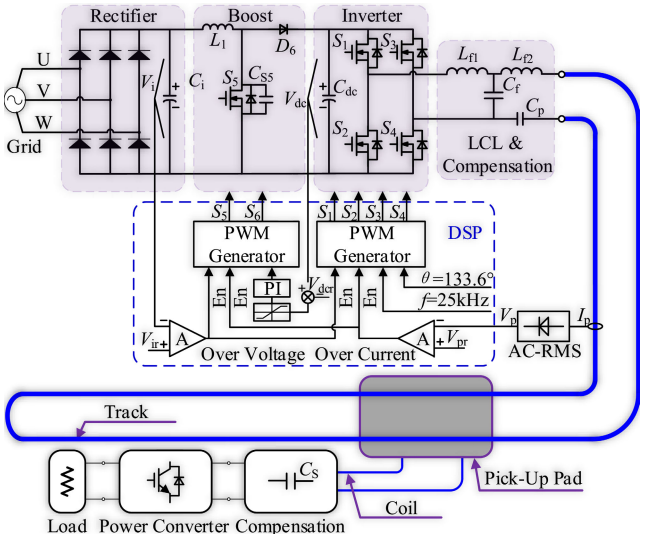

FIGURE 3. Proposed topology for dynamic IPT system.

to improve the efficiency and the reliability of the primary side of the dynamic IPT system. Dynamic IPT system must keep in the CC mode of the track because of the uncertain load characteristics. The H-bridge resonant inverter along with LCL network and series-series type capacitors C_p and C_s are shown in Fig. 4(a). L_{f1} is the inductance at the inverter side. L_{f2} is the inductance at the track side. C_f is the resonant capacitance at the primary side. The parasitic resistances of the LCL are assumed to be small, which can be neglected. The switching signals, electrical waveforms, and control signals of the H bridge are shown in Fig. 4(b).

The resonant frequency between L_{f1} and C_f is the same as the switching frequency ω. The conditions to reach the zero phase angle (ZPA) are given by

$$\omega^2 = \frac{1}{L_p C_p} \omega^2 = \frac{1}{L_{s1} C_{s1}}, \quad \text{and } \omega^2 = \frac{1}{L_{sn} C_{sn}}. \tag{1}$$

Here, L_{s1} to L_{sn} are compensated with C_{s1} to C_{sn}. As a result, capacitors $C_{s1} - C_{sn}$ and C_p completely compensate the leakage inductors no matter what happens to $R_{eq1} - R_{eqn}$ and mutual inductors M.

As shown in Fig. 4(b), V_{ac} is the output voltage of the inverter. The voltage pluse width θ is changed with S1-S4 phase shift modulation. According to Fourier's formula, V_{ac} can be expressed as

$$V_{ac}(t) = \sum_{n=1}^{\infty} \frac{4V_{dc}}{n\pi} \sin\left(\frac{n\theta}{2}\right) \cos\left[n\omega\left(t - \frac{\theta T}{4\pi}\right)\right] (n \text{is odd.}). \tag{2}$$

In most IPT studies, first harmonic approximation (FHA) is used to analyze the topology. The fundamental component of V_{ac} is given by

$$V_{ac1}(t) = \frac{4V_{dc}}{\pi} \sin\left(\frac{\theta}{2}\right) \cos\left[\omega\left(t - \frac{\theta}{4\pi} T\right)\right]. \tag{3}$$

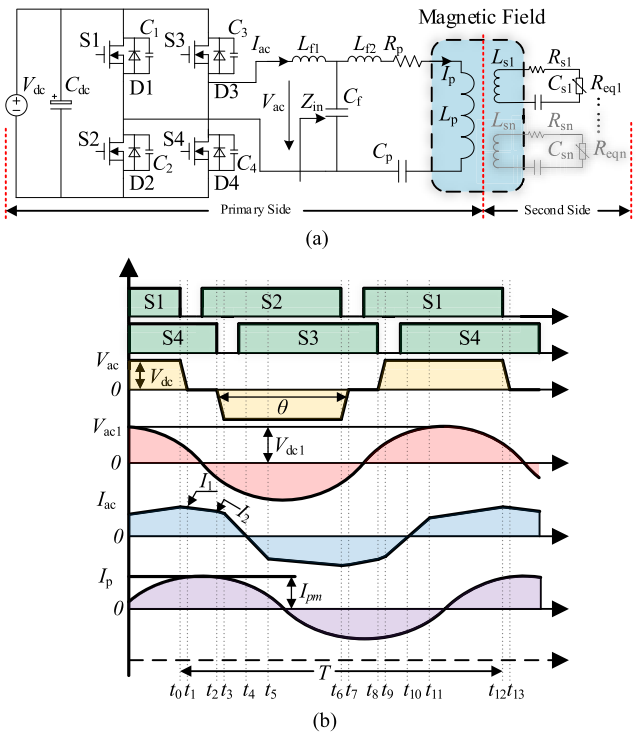

FIGURE 4. PWM voltage modulated description of the dynamic IPT system. (a) Primary inverter of the dynamic IPT system. (b) Inverter output voltage, track current, and switching signals.

The Z_{in} in frequency domain is given by

$$Z_{in} = j\omega L_{f1} + \left[\frac{1}{j\omega C_f} // \left(j\omega L_{f2} + R_{eq}\right)\right] \tag{4}$$

where R_{eq} is the equivalent impedance of the output port in LCL circuit. The conditions to realize ZPA and CC mode of the primary track are given by

$$L_{f1} = L_{f2}, \quad j\omega L_{f1} = \frac{1}{j\omega C_f}. \tag{5}$$

According to (1), (4), and (5), Z_{in} can be obtained the pure impedance characteristic and it is then given by

$$Z_{in} = \frac{\omega^2 L_{f1}^2}{R_{eq}}. \tag{6}$$

$\dot{V}_{ac1}$ is transformed to the primary track I_p using Norton's equivalent equation in frequency domain, which is given by

$$\dot{I}_p = \frac{4V_{dc}}{\pi\omega L_{f1}} \sin\left(\frac{\theta}{2}\right) \angle -90°. \tag{7}$$

Here, the $\dot{V}_{ac1}$ is defined as

$$\dot{V}_{ac1} = \frac{4V_{dc}}{\pi} \sin\left(\frac{\theta}{2}\right) \angle 0°. \tag{8}$$

Note that the fundamental voltage component V_{ac1} passes through the LCL networks and produces the current I_p in the track. However, other harmonic voltage components of V_{ac} produce large harmonic power circulation in LCL network and H bridge. To optimize this, the factor related to θ should be considered. THD of V_{ac} is introduced to measure the quality of V_{ac}.

$$THD_u = \frac{\left|V_{dc}\sqrt{\frac{\theta}{\pi}}\right|^2 - \left|\dot{V}_{ac1}\right|^2}{\left|\dot{V}_{ac1}\right|^2} = \frac{\pi^2\theta}{1440\sin^2\left(\frac{\theta}{2}\right)} 1 \tag{9}$$

where n is odd. $\dot{V}_{acn}$ is defined as

$$\dot{V}_{acn} = \frac{4V_{dc}}{n\pi} \sin\left(\frac{n\theta}{2}\right) \tag{10}$$

where V_{ac1} is defined as

$$V_{ac1} = \left|\dot{V}_{ac1}\right| = \frac{4V_{dc}}{\sqrt{2}\pi} \sin\left(\frac{\theta}{2}\right). \tag{11}$$

Combined with (9) and (11), the curves of the θ between the THD_u and V_{ac1} are shown in Fig. 5.

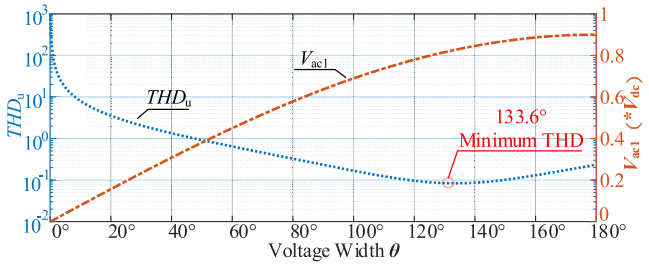

FIGURE 5. Curves of THDu and Vac1 with variable θ.

According to the characteristic shown in Fig. 5, big change of θ is needed to control the fluctuation of bus voltage in PWM based voltage control mode, which leads to a large THD_u value.

Furthermore, the output power of the H bridge is given by

$$P_H = \frac{(1+THD_u)\left|\dot{V}_{ac1}\right|^2}{Z_{in}} = (1+THD_u)P_{out} = V_{ac}I_{ac}. \tag{12}$$

Then, P_{out} is constant for the output power of LCL networks. I_{ac} is smaller with smaller THD_u and higher V_{ac}. According to the curves shown in Fig. 5, the THD_u has a minimum value of 0.084 when θ is 133.6 degrees. When θ is changed, THD_u is changed significantly. V_{ac1} is monotonously increasing with θ and it changes limitedly when the range of θ becomes small. For example, V_{ac1} changes slightly from 0.84 to 0.90 when θ is between 133.6° and 180°, while THD_u is changed from 0.084 to 0.233. It is significant that the change of θ for getting a constant voltage (CV) of V_{ac1} causes large harmonic components of V_{ac}, which reduces the efficiency and enlarge the voltage and current stresses of the device. Therefore, to optimize the output current of the H-bridge resonant inverter with minimized THD_u value, the voltage width θ of the output high frequency voltage is set as a fixed value of 133.6 degrees in the proposed two-stage IPT system. Instead of changing θ to get a CV of V_{ac1} in conventional dynamic IPT system, the proposed system introduces a boost converter in the front

to regulate and increases the input voltage in the H-bridge resonant inverter. According to (2), it also enhances V_{ac} in a reasonable condition to compensate the voltage loss caused by the reducing θ to implement the smaller I_{ac}.

B. DESIGN OF THE PROPOSED TWO-STAGE IPT SYSTEM

The boost converter is shown in Fig. 6. The filter capacitors of input and output are C_{dc} and C_i respectively. L_1 is used to smooth the current fluctuation caused by the voltage drop between V_{dc} and V_i. V_i is regulated by controlling the on-off of S_5.

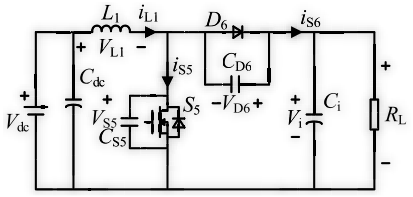

FIGURE 6. Boost regulator circuit.

To achieve the soft switching, the boost converter works in DCM. V_{dc} and V_i are considered to be constant due to the large capacitance value of C_{dc} and C_i. The key waveforms of the boost regulator are shown in Fig. 7. The boost regulator prefers to work in DCM. S_5 turns on and D_6 turns off in both zero-current-switching (ZCS) compared to continuous conduction mode (CCM). The interval $t_0 - t_4$ describes four stages of operation during one complete switching cycle in Fig. 7(b). T_b is defined as the time of one period, which is constant in this paper. D is defined as the ratio that is the conduction time divided by the period. D changes for regulating V_i, which is caused by the fluctuation of V_{dc}.

The switching mode is divided into four operating modes in one complete period in DCM mode.

Mode 1 $[t_0 - t_1]$: Current flows through S_5. The current of L_1 increases linearly and can be expressed as

$$i_{L1}(t) = \frac{V_{dc}}{L_1}(t - t_0) \tag{13}$$

where $i_{L(1)} = \frac{V_{dc}}{L_1} DT_b$.

Mode 2 $[t_1 - t_2]$: S_5 turns off with zero voltage switch (ZVS) at t_1 because of C_{S5}. D_6 turns on at the same time to pass inductive current i_{L1}. The current of L_1 decreases linearly and can be expressed as

$$i_{L1}(t) = i_{L(1)} - \frac{V_i - V_{dc}}{L_1}(t - t_1). \tag{14}$$

Mode 3 $[t_2 - t_3]$: i_{L1} equals to 0 at t_2. i_{L1} is then discharging C_{S5} and charging C_{D6}. A complete resonance period ends at t_3. The time duration of t_{23} can be given by

$$t_{23} = \pi\sqrt{2C_j L_1}. \tag{15}$$

Here, C_{S5} and C_{D6} are the junction capacitance of the MOSFET, which equal to C_j. Since the C_j of the switch is small, the resonant current through the switch is not large. S_5 turns on with zero current switch (ZCS) at t_3.

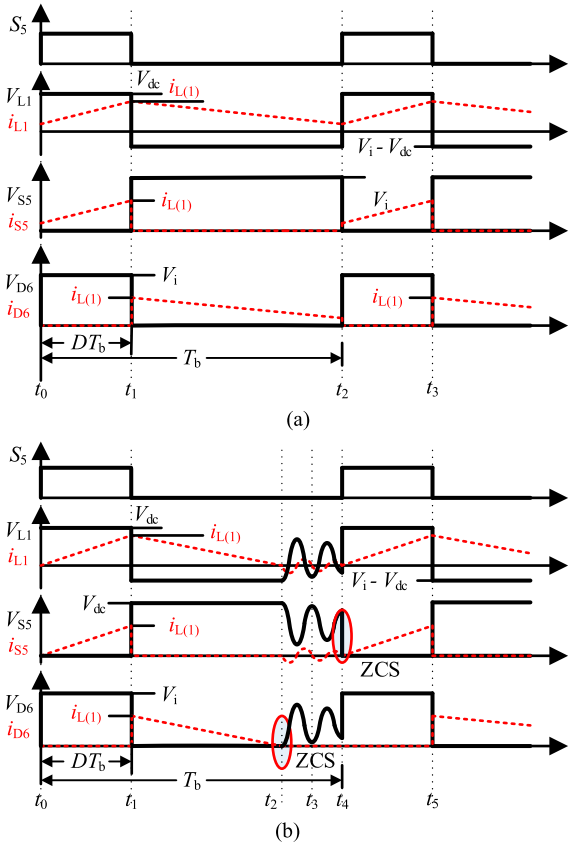

FIGURE 7. Key waveforms of the boost regulator. (a) CCM mode. (b) DCM mode.

Mode 4 $[t_3 - t_4]$:i_{L1} equals to 0 after half resonant period at t_3. The mode continues until the next circulation comes. The output power can be given by

$$P_{out} = \frac{1}{2}\frac{V_{dc}V_i^2}{L_1(V_i - V_{dc})}D^2 T_b. \tag{16}$$

The requirement of realizing DCM mode is given by

$$T_1 = \left(1 + \frac{V_{dc}}{V_i - V_{dc}}\right)DT_b < T_b. \tag{17}$$

The soft switching of the H-bridge resonant converter is analyzed in this part. The switching frequency equals the resonant frequency of the resonant network. $C_1 - C_4$ are the junction capacitance of S1-S4. The resonant topology has pure resistant characteristics according to (6). It can be equivalent to L_t, because the tank can be slightly inductive, which can better realize soft switching. The relation of $C_1 - C_4$ is given by

$$C_1 = C_2 = C_3 = C_4 = C. \tag{18}$$

Initially, S1 and S4 conduct at the same time until t_0. During the interval $t_0 < t < t_1$, S1 turns off causing I_{ac} passing to D2. As a result, I_{ac} charges C_1 and discharges C_3 with

zero voltage turning-off. The I_{ac} is approximately constant caused by L_t. The interval length $(t_0 - t_1)$ is given by

$$t_{01} = \frac{2CV_{dc}}{I_1}, \quad i_{ac}(t) = I_{ac}(t_0) = I_1. \tag{19}$$

Then, D2 is conducted because of the current flowing, which causes zero-voltage turn-on of S2. The dead time $t_{d(dead)}$ between S1 and S2 must also be longer than t_{01}. i_{ac} is the second primary current reflecting to the primary side and is given by

$$i_{ac}(t) = i_{sec}/K. \tag{20}$$

i_{sec} is the second primary current at the interval $t_1 < t < t_2$. K is the current gain of second side reflecting to the primary side. I_{ac} decreases to I_2 at the end of t_2. S4 is turning off with zero voltage switch with the condition when I_2 is positive. At the same time, I_{ac} charges C_4 and discharges C_3 at t_2. So the bigger θ is, the easier S4 realizes ZVS. C_3, C_4, and L_t are in series resonance due to phase-shifted duty-cycle loss. I_{ac} and the voltage of C_3 and C_4 are given by

$$\begin{aligned} i_{ac}(t) &= I_2\cos\omega_t(t - t_2), \quad V_{C4}(t) = Z_1 I_2 \sin\omega_t(t - t_2) \\ V_{C3}(t) &= V_{dc} - Z_1 I_2 \sin\omega_t(t - t_2). \end{aligned} \tag{21}$$

Here, the expressions of Z_1 and ω_t are given by

$$\omega_t = 1/\sqrt{2L_tC}, \quad Z_1 = \sqrt{L_t/(2C)}. \tag{22}$$

The interval $t_2 < t < t_3$ finishes with the voltage of C_4 rising to V_{dc}. The time of duration is given by

$$t_{23} = \frac{1}{\omega_1}\arcsin\frac{V_{dc}}{Z_1 I_1}. \tag{23}$$

D3 is then conducted with the current flowing. That causes zero-voltage turn-on of S3. The dead time $t_{d(dead)}$ between S3 and S4 must be longer than t_{23}.

The interval $t_0 < t < t_3$ shows the half period. The second half period of the cycle is similar. The soft switching condition is relevant to $t_{d(dead)}$, C, L_t, K, and i_{sec} according to the analysis above. The load is also the main issue for soft switching connected with the value of I_{ac}. The soft switching operation cannot be achieved when the load is light. This paper focuses on the condition from half load to full load to realize the soft switching of the H bridge.

III. DESIGN PROCESS AND CALCULATING EXAMPLE

A. PROPOSED SYSTEM DESIGN

From the above, a complete design example of this circuit is shown as follows.

1) According to [37], the voltage from the grid side to dc side is given by

$$V_{dc} = (1.35\text{-}1.41)\, V_{acin}. \tag{24}$$

The parameters of the boost converter are given in Table 3. P_{max} means the maximum power to realize the DCM in boost stage for the ZCS in boost stage design.

2) The aim of the proposed boost design is to determine the appropriate parameters of L_1 when V_i fluctuates. First of all, the boost converter needs to meet the requirements of voltage regulating range at specified output power in P_{out} according to (16). It is also expected to work in DCM to realize soft switching. (17) gives the conditions for realizing DCM.

TABLE 3. Experiment parameters of IPT system.

Symbol	Quantity	Value
V_{acin}	grid source	380 V ± 7% (AC)
V_{dc}	input voltage	470 V – 570 V (DC)
f_s	switch frequency	50 kHz
H	efficiency of the boost converter	≥95% (at ≥ 10% load)
V_i	output voltage	750 V
P_{out}	maximum power to realize the DCM	1500 W
C_j	junction capacity	200 pF

The data are plotted in Fig. 8 to deal with the parameter design for L_1 based on (16) and (17). The surface below the 1500 W plane meets the requirement of working in specific power output and DCM. i_{L1} gets smaller as L_1 gets bigger according to (13). L_1 equals to 400 μH from the above considerations.

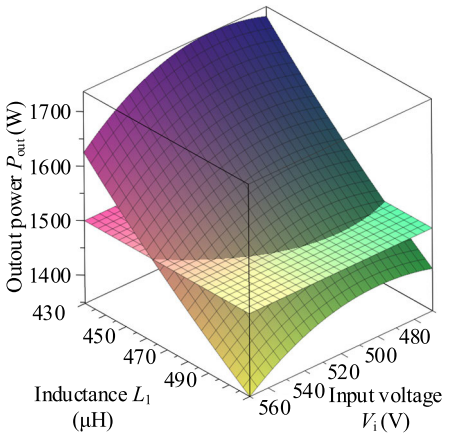

FIGURE 8. Calculated values of Pout with variable L_1 and V_i.

3) The inverter prefers to work at a θ of 133.6 degrees to get the smaller value of current I_{ac}. The root mean square of I_p is defined as 60 A according to the application requirement. The values of LCL networks can be calculated according to (5) and (7). They are verified for the realization of soft switching according to (22) shown in Table 4.

TABLE 4. Experiment parameters of IPT system.

Symbol	Value	Symbol	Value
L_{f1}	65 μH	L_{f2}	65 μH
C_f	620 nF	C	100 pF
t_d	1 μs	V_{dc}	750 V
f	25 kHz		

B. PROPOSED SYSTEM DESIGN

V_{out} with series- and series- compensations is given by

$$V_{out} = \left|\dot{V}_{out}\right| = \omega M I_p \tag{25}$$

I_p and ω are constant in CC mode. V_{out} is larger that can cause I_c smaller to reduce coil loss. M is therefore designed as large as possible with the consideration of surface effect and proximity effect.

According to the requirement for material handling, simplified mathematical model of track and coils in the IPT system is shown in Fig. 9. In this paper, it is worth noting that the system is used in industrial material handling. The vehicles have a fixed running track with relatively low speed (3 m/s at the highest). The magnetic field is distributed while it is in motion. So the magnetic field is relatively stationary in the application. In [2]–[5], the mutual inductance M is calculated at stationary for dynamic IPT system. Therefore, the influence of velocity on M is ignored in this paper.

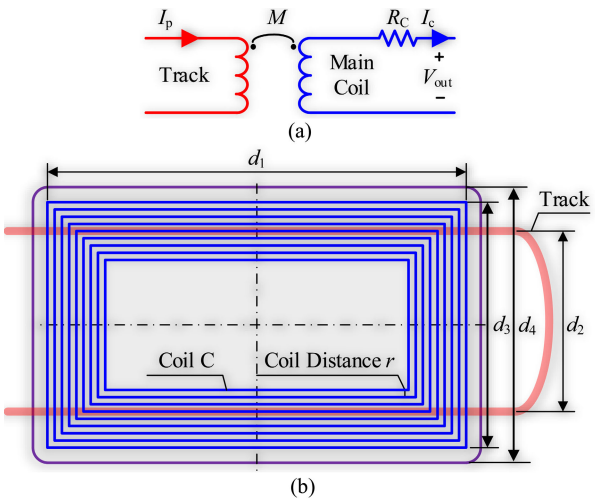

FIGURE 9. Magnetic field coupling model for parallel system. (a) Simplified circuit model; (b) Flat structure model.

M and R_c are the key factors for the applications shown in Fig. 9(a).

As shown in Fig. 9(b), the flux linkages of the two coils are the sum of the fluxes generated by the main and auxiliary tracks. The cutaway structure models with tracks and j-th coils are shown in Fig. 10.

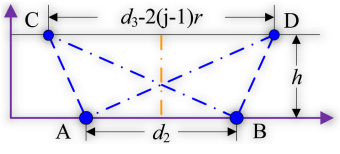

FIGURE 10. Cutaway structure models with track and j-th coil.

The magnetic flux produced by track A through the j-th coil area is given by

$$\begin{aligned}\phi_A &= \int_0^{d_1-2(j-1)r} dz \int_{L_{AC}}^{L_{AD}} \frac{\mu_0 I_P}{2\pi\rho} d\rho \\ &= \frac{\mu_0 I_P}{2\pi}\left[(d_1 - 2(j-1)r)\ln\frac{L_{AD}}{L_{AC}}\right].\end{aligned} \tag{26}$$

The magnetic flux produced by track B through the j-th coil is given by

$$\begin{aligned}\phi_B &= \int_0^{d_1-2(j-1)r} dz \int_{L_{BD}}^{L_{BC}} \frac{\mu_0 I_P}{2\pi\rho} d\rho \\ &= \frac{\mu_0 I_P}{2\pi}\left[(d_1 - 2(j-1)r)\ln\frac{L_{BC}}{L_{BD}}\right].\end{aligned} \tag{27}$$

The length values of L_{AD}, L_{AC}, L_{BC}, and L_{BD} are calculated by the Pythagorean Theorem shown in Fig. 10.

Furthermore, the total mutual inductance M_s between the track and the rectangular coils is given by

$$\begin{aligned}M_S &= \frac{\Psi_S}{I_P} \\ &= \frac{\mu_0}{\pi}\sum_{j=1}^{N}\left[(d_1 - 2(j-1)r)\ln\frac{h^2+[\frac{d_3-2(j-1)r+d_2}{2}]^2}{h^2+[\frac{d_3-2(j-1)r-d_2}{2}]^2}\right].\end{aligned} \tag{28}$$

N is the turns of the coils. h is the vertical distance between coils and track.

The limits of the coils with symmetrical structures are given by

$$d_2 + r\,(N-1) = d_3 \quad (N \le 25). \tag{29}$$

The direct current resistance R_{dcs} is calculated as follows:

$$R_{dcs} = \rho_{cu}\frac{2N\,(d_1 + d_3 - 2Nr)}{S_s}. \tag{30}$$

ρ_{cu} is the electrical resistivity and S_S is cross-sectional area of the coil.

The alternating current resistance R_{acs} considering the skin effect is then given by

$$R_{acs} = F_R R_{dcs}. \tag{31}$$

Here, F_R is given by the manufacturers.

Furthermore, r has minimum limited value considering the proximity and skin effects. According to (24) and (30), the coil transfer efficiency η_c is then given by

$$\eta_c = \frac{P_{in} - I_s^2 R_{acs}}{P_{in}} = 1 - \frac{P_{in} F_R R_{dcs}}{(\omega M I_p)^2}. \tag{32}$$

Here, P_{in} and I_s are the input power and current of the coils respectively.

As is shown in Table 5, the specific parameters of the coils are given accounting for the application. The coils are made of 700 strands Lizi wire with diameter of 0.1 mm per strand.

Combined with the calculating progress in section B, values of M and η_c with variable N, and r are shown in Fig. 11. From the results, the maximum value of M is

TABLE 5. Coils parameters.

Symbol	Value	Symbol	Value
d_1	300 mm	d_2	200 mm
d_4	350 mm	r	>= 4 mm
S_s	3 mm^2	h	15 mm
P_{in}	400 W	$\rho_{cu\ @80°C}$	2.2×10^{-8} Ω·m
F_R	1.25		

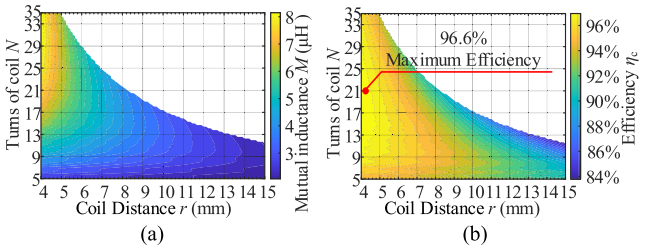

FIGURE 11. Calculated values of M and η_c with variable N and r. (a) M-N-r; (b) η_c-N-r.

8.4 μH. The maximum efficiency η_c is there 96.6%, which considers the copper loss of the coils. With the comprehensive consideration of the weight, cost, M and η_c. Coil parameters can be obtained as $N = 21$, $r = 4.2$ mm and $M = 6.6\mu$H respectively.

The 3D Maxwell FEA simulation is then used to optimize and analyze the calculated results. FEA simulation model of the track and the coil are shown in Fig. 12.

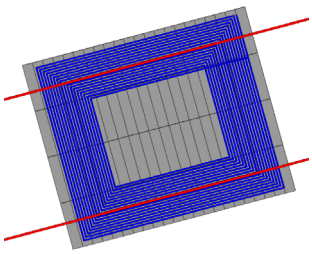

FIGURE 12. Finite element simulation model.

Ferrite PC40 strips are placed over the coils to optimize the magnetic circuit, reduce, and shield the magnetic field. They are close to the coil surface. The size of the stripe is 70 mm × 5 mm × 15 mm. The coils parameters with the FEM can be obtained as N=21, $r = 4.2$ mm, and $M = 6.5\mu$. η_c is then calculated as 94%.

Finally, the magnetic field distribution is evaluated by the simulation results. The magnetic field intensity of the coils is equally distributed, which is shown in Fig. 13 (a). The design of magnetic strips meets the requirement based on Fig. 13 (b). Fig. 13 (c) shows that magnetic field radiation satisfies the relevant standard of the International Commission on Non-Ionizing Radiation Protection (ICNIRP) under the working condition.

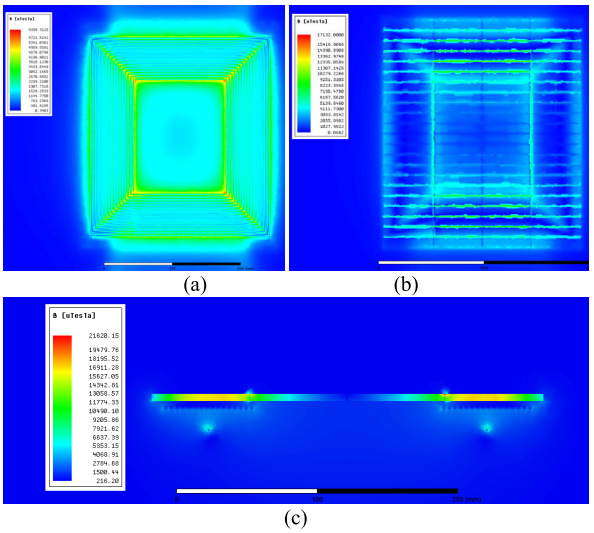

FIGURE 13. Simulation results of magnetic field. (a) The coil magnetic field distribution. (b) The stripes magnetic field distribution. (c) The vertical magnetic field distribution.

IV. SIMULATION AND EXPERIMENT VERIFICATION

A. SIMULATION VERIFICATION

The simulation platform of MATLAB is established to verify that THD_u of I_{ac} is the minimum when track current is constant compared to the voltage pulse width control. The value of I_{ac}, θ, and constant I_P with voltage pulse width control is shown in Fig. 14 when the source DC bus fluctuates in 800 W Load.

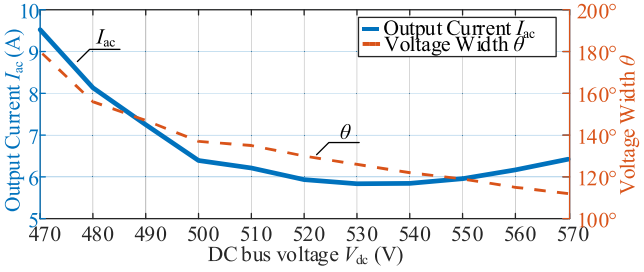

FIGURE 14. Simulation results of Iac, θ, and Vdc with voltage pulse width control.

θ keeps decreasing as V_{dc} increase. Meanwhile, the change trend of I_{ac} is the same as that of THD_u in Fig. 14. However, the amplitude of fundamental component of I_{ac} increases during the rise of V_{dc}. This leads to a slight difference in the trend of changes in I_{ac} and THD_u.

Simulation results of the H-bridge waveforms are presented in Fig. 15. The soft switching is realized in the device switches when V_{dc} equals 750 V with 400 W load, which is the worst conditions of the soft switching.

In order to verify the advantages of the proposed system, push-pull, boost with push-pull, full-bridge, and the proposed system are compared. The results of the voltage and current stresses, THD_u, and the efficiency are shown in Fig. 16. The simulation maintains the track current I_p of 60 A,

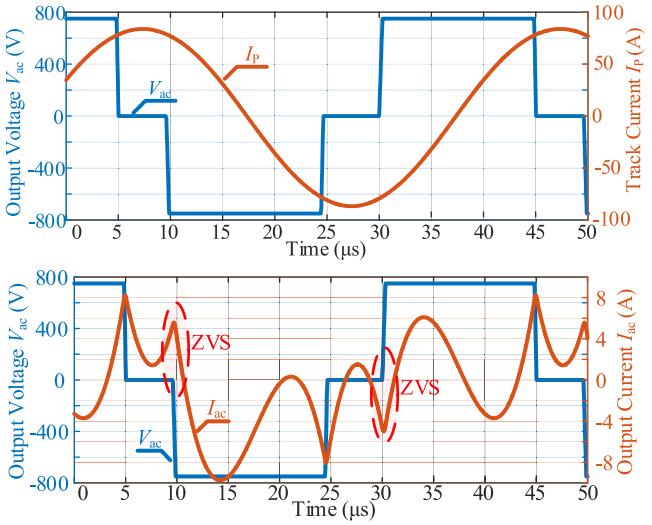

FIGURE 15. Main waveforms simulation of the inverter in 400 W load.

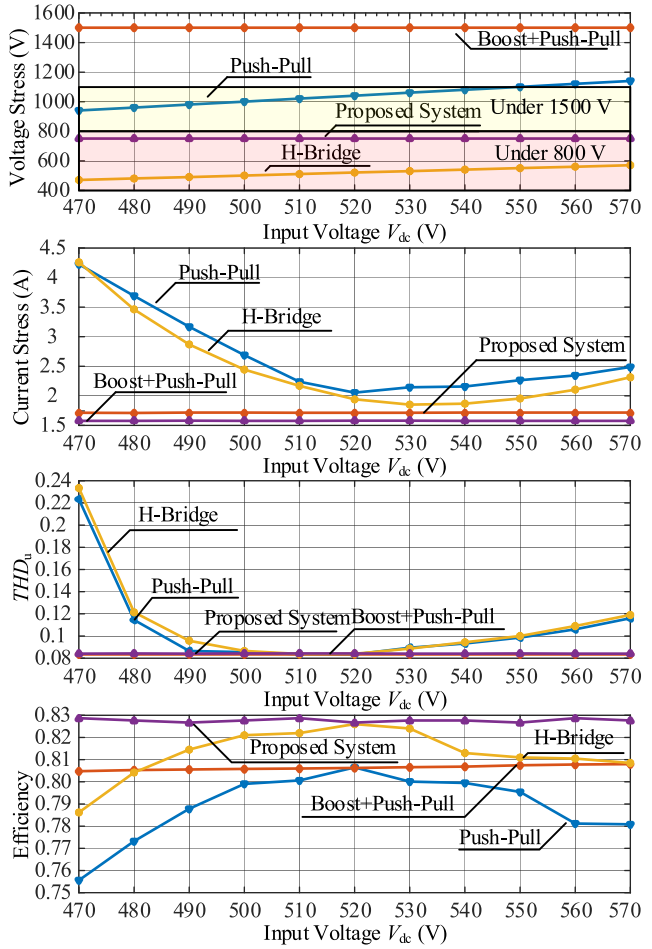

FIGURE 16. Simulation comparison of the proposed system, push-pull, boost with push-pull, H-bridge, and the proposed system.

the 800 W output power, and the input voltage fluctuation of 480 V – 570 V.

Through the comparison of voltage stresses, the voltage stresses of push-pull and boost + push-pull are more than 1500 V. The proposed system has the constant voltage stress of about 800 V. In terms of current stress and THD_u, the proposed system has small values of about 1.6 A and 0.086 respectively. As a result, the highest efficiency is obtained in the proposed system of about 82%.

The resonant capacitor C_f flows large current and it is more sensitive to parameter drift. The effects of parameter drift of C_f are shown in Table 6. The results show that little effect was produced on the system when the parameter drift is ±2%. However, when the parameter deviation increases over ±5%, the parameter drift causes large track current deviation, which increases the output current of the H bridge. As a result, the system efficiency drops sharply, related protection may be activated when the drift is too large. To solve this problem, series and parallel combinations of ceramic capacitors or film capacitors can be employed in practical application. The other parameters will be considered in our further research.

TABLE 6. Effect of parameter drift of Cf in the proposed system.

C_f (nF)	I_P (A)	I_{ac} (A) (800 W)	Efficiency
682 (+10%)	67.03	8.35	77.8%
651 (+5%)	63.05	5.789	80.6%
632 (+2%)	61.32	5.114	82.5%
626 (+1%)	60.81	5.04	82.7%
620 (0%)	60.28	5.015	82.8%
614 (-1%)	59.75	5.051	82.5%
608 (-2%)	59.21	5.148	82.3%
589 (-5%)	57.53	5.78	80.8%
558 (-10%)	54.95	7.439	78.1%

B. EXPERIMENT VERIFICATION

An experimental prototype was built using the design parameters given in Table 3, 4, and 5. Fig. 17 (a) shows a whole prototype system, with the proposed system in the primary side shown in Fig. 17 (b), along with the pick-up pad shown in Fig. 17 (c) for each 400 W output.

Voltage pulse-width control was verified in this prototype for comparison. The principles of design is that the minimum input source voltage can get the designed track current. The width voltage pulse-width was decreasing with the source voltage increasing. Fig. 18 shows the waveforms of V_{ac}(CH1) and I_{ac} (CH2) at half and full load at fixed I_p(CH3) with different V_{dc} in PWM voltage width control. The track kept 60 Arms with the voltage fluctuation from 470V to 570V. There was a noticeable change in I_{ac} with constant output power P and track cuttent I_p.

In the proposed system, Fig. 19(a) shows the main H-bridges inverter waveforms. I_{ac} was constant with the THD_u of 0.084 when the V_{dc} changes. It is samller than the H bridge with voltage width control. Meanwhile, the waveforms were the same as the simulation shown in Fig. 15 and verified the ZVS realization. Fig. 19(b) shows the main boost stage waveforms, which verified DCM and ZCS shown in Fig. 7(b). There was basically no voltage spikes leading to small stresses in the main switches.

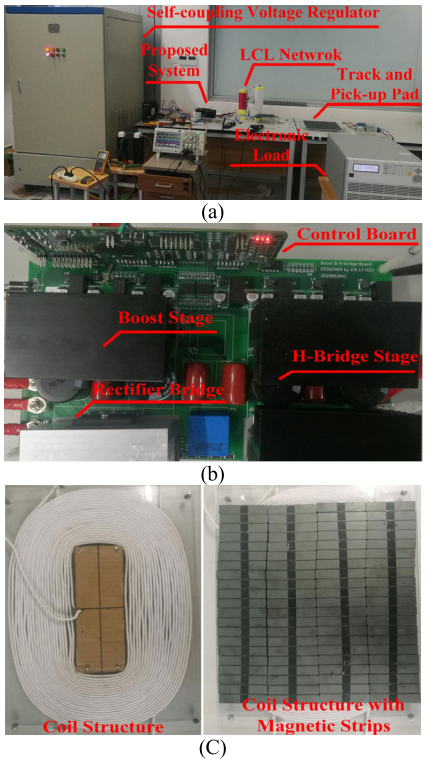

FIGURE 17. Experimental platform of IPT system. (a) Experimental panorama of the prototype. (b) The system of the primary side. (c) The pick up pad.

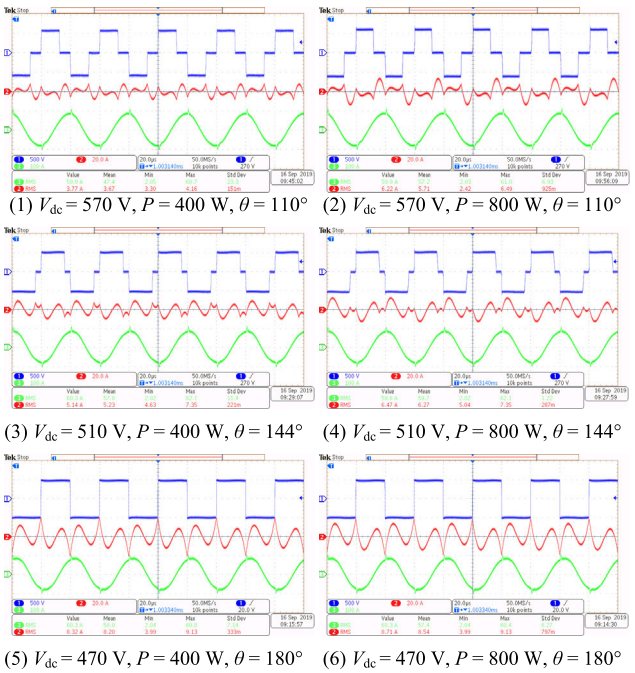

FIGURE 18. Main experimental waveforms of H-bridge inverter using voltage pulse width control with different shift angles and load (CH1:500 V/div, CH2:20 A/div, CH3:100 A/div, Time:20 μs/div).

Table 7 shows the data of I_{ac} with the width voltage pulse-width changing. The range with variation in I_{ac} was at least 30% with the at least 2.6 times change in THD_u.

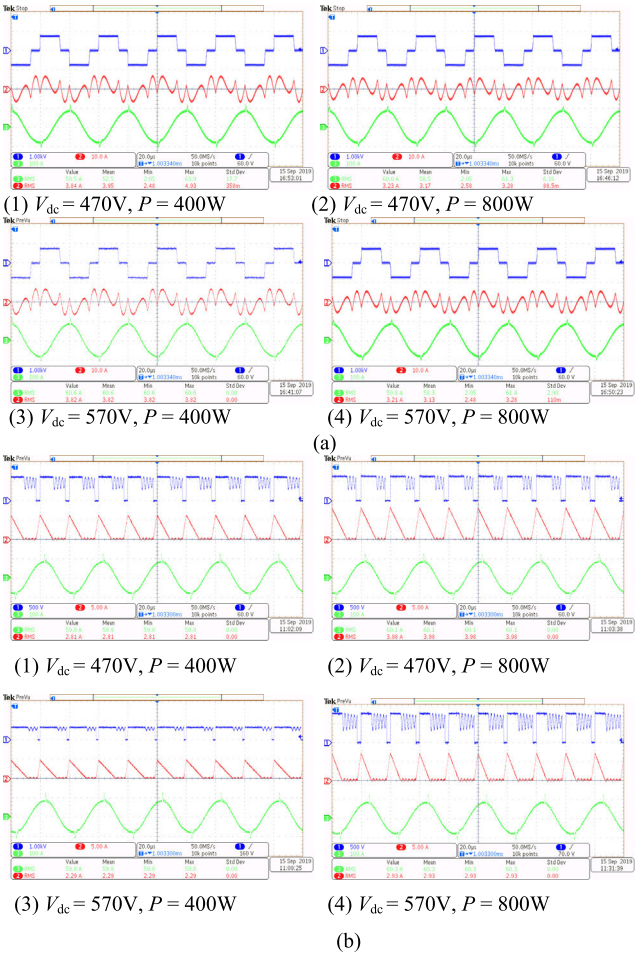

FIGURE 19. Experimental waveforms of the proposed system of 133.6 degrees of shifted angles. (a) Waveforms of Vac(CH1), Iac(CH2), and Ip(CH3) with half load (CH1:1000 V/div, CH2:10 A/div, CH3:100 A/div, Time:20 μs/div). (b) Waveforms of VS5, IL1 with full load and half load.

TABLE 7. Experimental data of voltage width control method.

V_{dc} (V)	θ (°)	THD_u	V_{ac1} (V)	I_{ac} (A) (400 W / 800 W)
470	180	0.23	423	8.32/8.71
490	154	0.11	425	6.70/7.16
510	144	0.09	425	5.14/6.47
530	126	0.087	421	3.90/5.07
550	115	0.10	423	3.85/4.98
570	110	0.12	421	3.77/6.22

This variation of I_{ac} directly affected the efficiency of the inverter. V_{ac1} is nearly the same, which shows a good regulation of realizing constant I_p. The data variation was nearly the same as the simulation shown in Fig. 14, which shows a good agreement with the theoretical analysis.

Table 8 shows the data of I_{ac} with the proposed system. The I_{ac} is nearly constant. V_{ac1} is higher than the H bridge with voltage width control. I_{ac} keeps the same because of the fixed θ and input DC bus voltage of the inverter.

TABLE 8. Experimental data of proposed method.

V_{dc} (V)	θ (°)	THD_u	V_{ac1} (V)	I_{ac} (A) (400 W / 800 W)
470	133	0.085	630	3.23/3.84
490	133	0.085	630	3.22/3.83
510	133	0.085	630	3.23/3.84
530	133	0.085	630	3.21/3.82
550	133	0.085	630	3.22/3.83
570	133	0.085	630	3.21/3.82

Fig. 20 shows the efficiency curve of the proposed system and the voltage pulse-width control system with variation of the input voltage from V_{dc} to rectifier load. It keeps the same regulating source range, mutual inductor, and load. The proposed system has the maximum loss reduction of 4% in 800 W load than the voltage pulse-width control. It also has the smaller range of efficiency variation of 2% compared to a H bridge with PWM control method system of which was 4.6%. Furthermore, the efficiency was higher with the increase of the load from 400 W to 800 W.

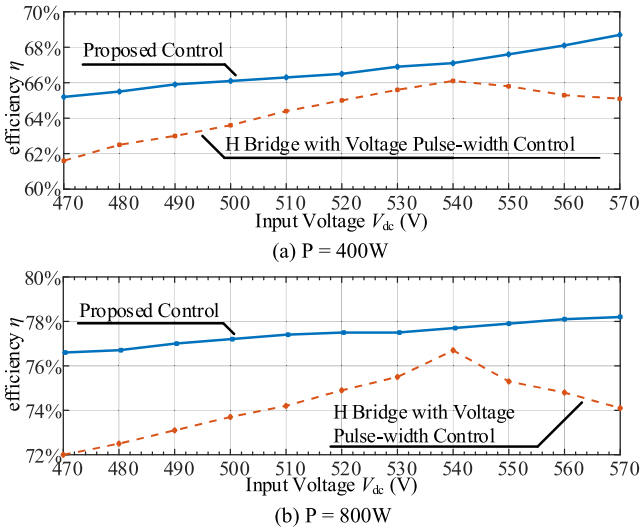

FIGURE 20. Efficiency curve of voltage pulse-width control and the proposed system with the variation of the input voltage.

V. CONCLUSION

In this paper, the method and design of a proposed IPT system for dynamic industrial material handling application is presented. The H-bridge power circulation is affected by the change of the input voltage. Therefore, THD_u of the H-bridge current is researched as well as the soft switching condition. The boost regulator in DCM mode is introduced to optimize the power circulation. The DC bus voltage is regulated to be constant and higher to realize the CC mode and reduce the I_{ac}. The coupling mechanisms is designed with the help of FEA simulation. The experimental results show that the efficiency reaches over efficiency of 76% at 800 W with the 15 mm air gap, and the proposed system has smaller THD_u. Compared to the H bridge with the voltage pulse-width control, the proposed system has the maximum loss reduction of 4.6% with smaller efficiency variation of 2%. The experimental results show a good agreement with the analyses. To further improve the efficiency of the whole system, the below approaches can be considered in our future work as: 1) The physical magnetic circuit-coupling model can be improved with the larger mutual inductance and more evenly distributed magnetic field. 2) The post-regulation circuit in the secondary side can be optimized to reduce the current and voltage stress of the switch devices, thus the overall switching loss can be reduced. 3) The wide bandgap devices such as SiC and GaN can be selected to reduce the conduction and switching losses of the switch devices. These methods will be considered in our future research.

REFERENCES

[1] F. Lu, H. Zhang, C. Zhu, L. Diao, M. Gong, W. Zhang, and C. C. Mi, "A tightly coupled inductive power transfer system for low–voltage and high–current charging of automatic guided vehicles," *IEEE Trans. Ind. Electron.*, vol. 66, no. 9, pp. 6867–6875, Sep. 2019.

[2] F. Lu, Y. Zhang, H. Zhang, C. Zhu, L. Diao, M. Gong, W. Zhang, and C. Mi, "A low–voltage and high–current inductive power transfer system with low harmonics for automatic guided vehicles," *IEEE Trans. Veh. Technol.*, vol. 68, no. 4, pp. 3351–3360, Apr. 2019.

[3] A. Zaheer, M. Neath, H. Z. Z. Beh, and G. A. Covic, "A dynamic EV charging system for slow moving traffic applications," *IEEE Trans. Transport. Electrific.*, vol. 3, no. 2, pp. 354–369, Jun. 2017.

[4] A. Zaheer, G. A. Covic, and D. Kacprzak, "A bipolar pad in a 10-kHz 300-W distributed IPT system for AGV applications," *IEEE Trans. Ind. Electron.*, vol. 61, no. 7, pp. 3288–3301, Jul. 2014.

[5] M. L. G. Kissin, H. Hao, and G. A. Covic, "A practical multiphase IPT system for AGV and roadway applications," in *Proc. IEEE Energy Convers. Congr. Expo.*, Sep. 2010, pp. 1844–1850.

[6] R. Ruffo, V. Cirimele, M. Diana, M. Khalilian, A. L. Ganga, and P. Guglielmi, "Sensorless control of the charging process of a dynamic inductive power transfer system with an interleaved nine–phase boost converter," *IEEE Trans. Ind. Electron.*, vol. 65, no. 10, pp. 7630–7639, Oct. 2018.

[7] G. A. Covic and J. T. Boys, "Inductive power transfer," *Proc. IEEE*, vol. 101, no. 6, pp. 1276–1289, Jun. 2013.

[8] M. Budhia, G. A. Covic, and J. T. Boys, "Design and optimization of circular magnetic structures for lumped inductive power transfer systems," *IEEE Trans. Power Electron.*, vol. 26, no. 11, pp. 3096–3108, Nov. 2011.

[9] M. Borage, S. Tiwari, and S. Kotaiah, "LCL–T resonant converter with clamp diodes: A novel constant–current power supply with inherent constant–voltage limit," *IEEE Trans. Ind. Electron.*, vol. 54, no. 2, pp. 741–746, Apr. 2007.

[10] C.-S. Wang, G. Covic, and O. Stielau, "Investigating an LCL load resonant inverter for inductive power transfer applications," *IEEE Trans. Power Electron.*, vol. 19, no. 4, pp. 995–1002, Jul. 2004.

[11] L. J. Chen, J. T. Boys, and G. A. Covic, "Power management for multiple–pickup IPT systems in materials handling applications," *IEEE J. Emerg. Sel. Topics Power Electron.*, vol. 3, no. 1, pp. 163–176, Mar. 2015.

[12] Y. Li, R. Mai, L. Lu, and Z. He, "Active and reactive currents decomposition–based control of angle and magnitude of current for a parallel multiinverter IPT system," *IEEE Trans. Power Electron.*, vol. 32, no. 2, pp. 1602–1614, Feb. 2017.

[13] Y. Li, J. Hu, F. Chen, S. Liu, Z. Yan, and Z. He, "A new-variable-coil-structure-based IPT system with load–independent constant output current or voltage for charging electric bicycles," *IEEE Trans. Power Electron.*, vol. 33, no. 10, pp. 8226–8230, Oct. 2018.

[14] H. Hao, G. A. Covic, and J. T. Boys, "An approximate dynamic model of LCL-*T*-based inductive power transfer power supplies," *IEEE Trans. Power Electron.*, vol. 29, no. 10, pp. 5554–5567, Oct. 2014.

[15] F. Lu, H. Zhang, H. Hofmann, W. Su, and C. C. Mi, "A dual–coupled LCC–compensated IPT system with a compact magnetic coupler," *IEEE Trans. Power Electron.*, vol. 33, no. 7, pp. 6391–6402, Jul. 2018.

[16] S.-J. Huang, T.-S. Lee, and T.-H. Huang, "Inductive power transfer systems for pt–based ozone–driven circuit with flexible capacity operation and frequency–tracking mechanism," *IEEE Trans. Ind. Electron.*, vol. 61, no. 12, pp. 6691–6699, Dec. 2014.
[17] S. Samanta and A. K. Rathore, "Analysis and design of load–independent ZPA operation for P/S, PS/S, P/SP, and PS/SP tank networks in IPT applications," *IEEE Trans. Power Electron.*, vol. 33, no. 8, pp. 6476–6482, Aug. 2018.
[18] S. Samanta and A. K. Rathore, "Small signal modeling and control of parallel–series/series resonant converter for wireless inductive power transfer," in *Proc. IEEE Transport. Electrific. Conf. Expo (ITEC)*, Jun. 2018.
[19] X. Qu, Y. Jing, H. Han, S.-C. Wong, and C. K. Tse, "Higher order compensation for inductive-power-transfer converters with constant–voltage or constant–current output combating transformer parameter constraints," *IEEE Trans. Power Electron.*, vol. 32, no. 1, pp. 394–405, Jan. 2017.
[20] J. Lu, G. Zhu, D. Lin, S.-C. Wong, and J. Jiang, "Load–independent voltage and current transfer characteristics of high–order resonant network in IPT system," *IEEE J. Emerg. Sel. Topics Power Electron.*, vol. 7, no. 1, pp. 422–436, Mar. 2019.
[21] O. Knecht and J. W. Kolar, "Performance evaluation of series–compensated IPT systems for transcutaneous energy transfer," *IEEE Trans. Power Electron.*, vol. 34, no. 1, pp. 438–451, Jan. 2019.
[22] Y. Chen, B. Yang, Z. Kou, Z. He, G. Cao, and R. Mai, "Hybrid and reconfigurable IPT systems with high–misalignment tolerance for constant–current and constant–voltage battery charging," *IEEE Trans. Power Electron.*, vol. 33, no. 10, pp. 8259–8269, Oct. 2018.
[23] L. Chen, G. R. Nagendra, J. T. Boys, and G. A. Covic, "Double–coupled systems for IPT roadway applications," *IEEE J. Emerg. Sel. Topics Power Electron.*, vol. 3, no. 1, pp. 37–49, Mar. 2015.
[24] H. Hao, G. A. Covic, and J. T. Boys, "A parallel topology for inductive power transfer power supplies," *IEEE Trans. Power Electron.*, vol. 29, no. 3, pp. 1140–1151, Mar. 2014.
[25] K. Aditya, S. S. Williamson, and V. K. Sood, "Impact of zero-voltage switching on efficiency and power transfer capability of a series-series compensated IPT system," in *Proc. IEEE Transp. Electrific. Conf. (ITEC-India)*, Dec. 2017, pp. 1–7.
[26] A. Safaee and K. Woronowicz, "Time–domain analysis of voltage–driven series–series compensated inductive power transfer topology," *IEEE Trans. Power Electron.*, vol. 32, no. 7, pp. 4981–5003, Jul. 2017.
[27] T. Mishima and E. Morita, "High–frequency bridgeless rectifier based ZVS multiresonant converter for inductive power transfer featuring high–voltage GaN–HFET," *IEEE Trans. Ind. Electron.*, vol. 64, no. 11, pp. 9155–9164, Nov. 2017.
[28] J. M. Arteaga, S. Aldhaher, G. Kkelis, C. Kwan, D. C. Yates, and P. D. Mitcheson, "Dynamic capabilities of multi–MHz inductive power transfer systems demonstrated with batteryless drones," *IEEE Trans. Power Electron.*, vol. 34, no. 6, pp. 5093–5104, Jun. 2019.
[29] G. Kkelis, D. C. Yates, and P. D. Mitcheson, "Class–E half–wave zero dv/dt rectifiers for inductive power transfer," *IEEE Trans. Power Electron.*, vol. 32, no. 11, pp. 8322–8337, Nov. 2017.
[30] A. Trigui, S. Hached, F. Mounaim, A. C. Ammari, and M. Sawan, "Inductive power transfer system with self–calibrated primary resonant frequency," *IEEE Trans. Power Electron.*, vol. 30, no. 11, pp. 6078–6087, Nov. 2015.
[31] A. Abdolkhani, A. P. Hu, and J. Tian, "Autonomous polyphase current–fed push–Pull resonant converter based on ring coupled oscillators," *IEEE J. Emerg. Sel. Topics Power Electron.*, vol. 3, no. 2, pp. 568–576, Jun. 2015.
[32] A. Kamineni, G. A. Covic, and J. T. Boys, "Self–tuning power supply for inductive charging," *IEEE Trans. Power Electron.*, vol. 32, no. 5, pp. 3467–3479, May 2017.
[33] J. Tian and A. P. Hu, "A DC-voltage-controlled variable capacitor for stabilizing the ZVS frequency of a resonant converter for wireless power transfer," *IEEE Trans. Power Electron.*, vol. 32, no. 3, pp. 2312–2318, Mar. 2017.
[34] R. Bosshard and J. W. Kolar, "Multi–objective optimization of 50 kW/85 kHz IPT system for public transport," *IEEE J. Emerg. Sel. Topics Power Electron.*, vol. 4, no. 4, pp. 1370–1382, Dec. 2016.
[35] H. Z. Z. Beh, M. J. Neath, J. T. Boys, and G. A. Covic, "An alternative IPT pickup controller for material handling using a current doubler," *IEEE Trans. Power Electron.*, vol. 33, no. 12, pp. 10135–10147, Feb. 2018.
[36] V. Prasanth and P. Bauer, "Distributed IPT systems for dynamic powering: Misalignment analysis," *IEEE Trans. Ind. Electron.*, vol. 61, no. 11, pp. 6013–6021, Nov. 2014.
[37] Z.-J. Fang, C. Chen, S.-X. Duan, C.-D. Ren, and T. Cai, "Performance analysis and capacitor design of three-phase uncontrolled rectifier in slightly unbalanced grid," *IET Power Electron.*, vol. 8, no. 8, pp. 1429–1439, Aug. 2015.

JUNKUN ZHANG was born in Hubei, China, in 1992. He received the B.S. degree from Hubei Polytechnic University, Huangshi, China, and the M.S. degree from the Wuhan University of Technology, Wuhan, China, in 2014 and 2017, respectively, all in electrical engineering. He is currently pursuing the Ph.D. degree with Hunan University, Changsha, China. In 2017, he joined the Institute of New Energy, Wuhan, China, where he is currently a Technique Supporting Executive. His research interests include inductive power transfer technology and dc–dc converters.

ZHIXING HE (Member, IEEE) was born in Hunan, China, 1989. He received the B.S. degree in information science and engineering from Central South University, Changsha, China, in 2011, and the Ph.D. degree in electrical engineering from Hunan University, Changsha, in 2017. He was a Postdoctoral Researcher with Hunan University, China, from 2017 to 2018, where he has been an Associate Professor with the College of Electrical and Information Engineering. His research interests include power electronics, medium voltage dc conversion, model predictive control, and modular multilevel converter.

AN LUO (Senior Member, IEEE) was born in Changsha, China, in 1957. He received the B.S. and M.S. degrees in industrial automation from Hunan University, Changsha, in 1982 and 1986, respectively, and the Ph.D. degree in fluid power transmission and control from Zhejiang University, Hangzhou, China, in 1993. From 1996 to 2002, he was a Professor with Central South University. Since 2003, he has been a Professor with the College of Electrical and Information Engineering, Hunan University, where he also serves as the Chief of National Electric Power Conversion and Control Engineering Technology Research Center. His research interests mainly include distributed generation, microgrid, and power quality. He was elected to the Chinese National Academy of Engineering (CNAE), in 2015, the highest honor for scientists and engineers in China. He was a recipient of Highly Prestigious China National Science and Technology Awards, in 2006, 2010, and 2014.

YANG LIU was born in Hunan, China, 1997. He received the B.S. degree in electrical engineering and its automation from Hunan University, Changsha, in 2018, where he is currently pursuing the M.S. degree in electrical engineering with the College of Electrical and Information Engineering. His main research interests include power electronics and medium voltage dc conversion.

GUOZHEN HU was born in Hubei, China, in 1979. He received the Ph.D. degree from the Huazhong University of Science and Technology, Wuhan, China, in 2012. He is currently a Professor with Hubei Polytechnic University, Huangshi, China. His current research interests include the modeling and control of wireless power transmission of contactless power supply systems.

XUE FENG received the Ph.D. degree in electrical and electronic engineering from Nanyang Technological University, in June 2016. Her specialization is on energy storage system modeling and control for renewable energy systems and electric vehicles. During her course of Ph.D. study from 2011 to 2015, she was also involved in electric vehicle research with TUM CREATE. She joined Land Transport Authority of Singapore and worked in e-mobility office, from September 2015 to June 2017. Since September 2016, she has been working as an Assistant Professor with Singapore Institute of Technology. Her job scope in LTA involved project management and coordination for EV related projects, technical consultation for EV charging infrastructure development, formulation of new research directions and policy making for better introduction of EVs. Her research interests include microgrid operation and planning, integration of distributed resources, and energy storage system modeling, planning, and control.

LEI WANG (Member, IEEE) received the B.Sc. degree in electrical and electronics engineering from the University of Macau (UM), Macao, China, in 2011, the M.Sc. degree in electronics engineering from the Hong Kong University of Science and Technology (HKUST), Hong Kong, China, in 2012, and the Ph.D. degree in electrical and computer engineering from UM, in 2017.

He was a Postdoctoral Fellow with the Power Electronics Laboratory, UM, from January 2017 to February 2019. He was a Visiting Fellow with the Department of Electrical and Computer Engineering, University of Auckland, from February 2019 to August 2019. In 2019, he joined the College of Electrical and Information Engineering, Hunan University, Changsha, China, where he is currently a Full Professor. He has authored one Springer books, three patents (USA and China) and over 30 journal articles and conference papers. He received the Champion Award in the Schneider Electric Energy Efficiency Cup, Hong Kong, in 2011, and the Macao Science and Technology R&D Award for Postgraduates (Ph.D.), in 2018.